# Ultrafast all-optical quantum control of magnetization dynamics

Na Wu [a,b], Shengjie Zhang [a,b], Yaxian Wang [a,*], Sheng Meng [a,b,c,*]

[a] *Beijing National Laboratory for Condensed Matter Physics and Institute of Physics, Chinese Academy of Sciences, Beijing 100190, China*
[b] *School of Physical Sciences, University of Chinese Academy of Sciences, Beijing 100190, China*
[c] *Songshan Lake Materials Laboratory, Dongguan, Guangdong 523808, China*

## ARTICLE INFO

Commissioning Editor: P. Hvoje

## ABSTRACT

With the development of laser and magneto-optical technology and the discovery of a broad range of magnetic quantum materials exhibiting exotic properties and new physics, ultrafast magnetization dynamics has become increasingly appealing to advanced magnetic information technology. Furthermore, manipulating magnetization *via* light provides insights into interactions among multiple degrees of freedom in condensed matters and has revealed a wide range of nonequilibrium phenomena. In this minireview, we first present the theoretical considerations of ultrafast magnetization dynamics from both classical and *ab initio* points of view. We then discuss several aspects of state-of-the-art experimental studies on light-induced magnetization dynamics in various materials, including ultrafast demagnetization and magnetization reversal, as well as coherent-phonon-driven magnetization precession and phase transitions. In particular, we highlight the role of light-induced phonons from some recent work in the latter two aspects, providing a completely new perspective as well as an alternative approach for optical control of magnetization dynamics. As a powerful means of dynamical control and thanks to the progress and advances of experimental techniques, all-optical quantum manipulation of emergent materials is becoming one of the most far-reaching frontier research areas of ultrafast sciences.

## 1. Introduction

### 1.1. Significance of ultrafast optical control of magnetization dynamics

As an essential member of quantum materials hosting multiple degrees of freedom (charge, spin, lattice, *etc.*), magnetic materials have a profound impact on the exploration of fundamental physical concepts and emerging phenomena in condensed matter physics, as well as the design of functionalized devices [1–11]. Meanwhile, the recent two decades have witnessed tremendous experimental development (*e.g.* time-resolved magneto-optic techniques, time- and spin-resolved photoemission measurements, time-resolved X-ray diffraction, X-ray magnetic circular dichroism, *etc.*) and theoretical progress (*e.g.* phenomenological three-temperature model combined with the Landau–Lifshitz–Gilbert equation, *ab initio* methods including the real-time time-dependent density functional theory, *etc.*) aiming to characterize the fundamental interactions for dynamical magnetization phenomena. Among them, advanced laser technology with precise phase and frequency control [11–16], in a combination of time-resolved magneto-optical techniques has made it possible to realize ultrafast characterization, probe, and control of transient magnetization on the femtosecond or even attosecond timescale [11,17–21], and evolves to a rich field of *ultrafast magnetism* [22]. It includes a broad spectrum of

---

* Corresponding authors at: Beijing National Laboratory for Condensed Matter Physics and Institute of Physics, Chinese Academy of Sciences, Beijing 100190, China.
*E-mail addresses:* yaxianw@iphy.ac.cn (Y. Wang), smeng@iphy.ac.cn (S. Meng).
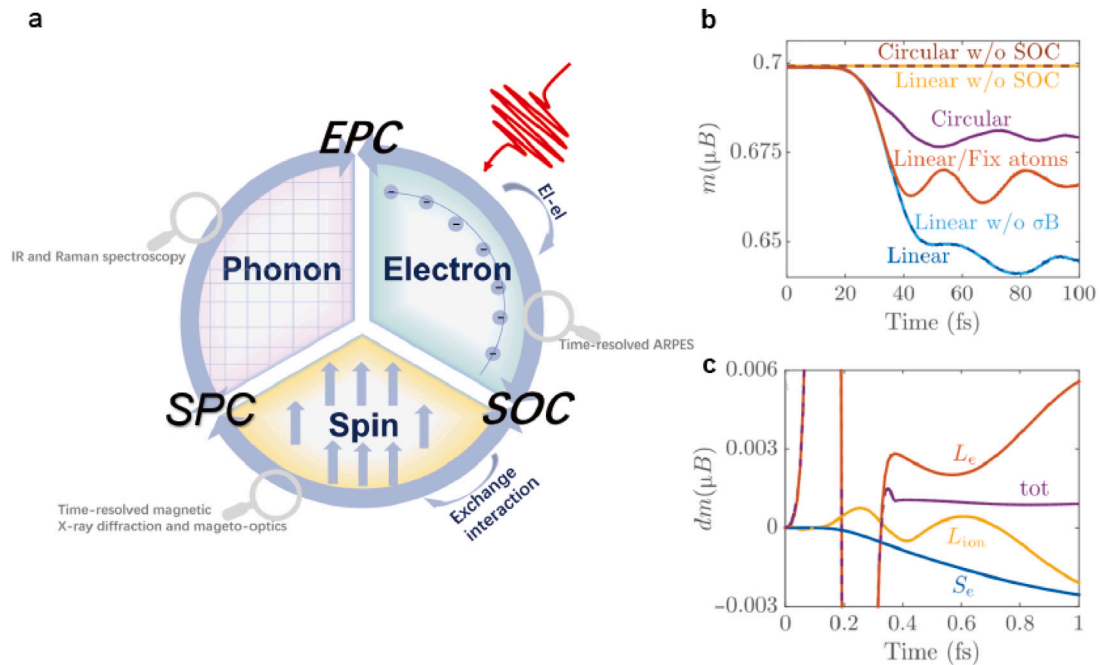
**Fig. 1.** Coupling between spin and other degrees of freedom. (a) Interactions among multiple degrees of freedom in condensed matter. Here, the spin–orbit coupling (SOC) interaction represents the coupling between spin and electron, spin–phonon coupling (SPC) refers to the interaction between spin and phonon, and EPC is the coupling between electron and phonon. (b) Demagnetization of bulk Ni highlighting the effect of light polarization, SOC, the light–spin interaction ($\hat{\sigma} \cdot \boldsymbol{B}$), and the phonons from theoretical calculations. The six cases are: (i) linear polarized laser, (ii) linear polarized laser without the $\hat{\sigma} \cdot \boldsymbol{B}$ term, (iii) linear polarized laser without phonons, (iv) circular polarized laser, (v) linear and (vi) circular polarized laser without including SOC. (c) Temporal evolution of electron spin $S_e$, electron orbital angular momentum $L_e$, ion orbital angular momentum $L_{ion}$, and the total angular momentum *tot* for a two-atom Ni dimer. (b) and (c) are reproduced from Ref. [23].

transient magnetization dynamics, such as ultrafast demagnetization, magnetization precession, magnetization reversal, magnetic phase transition, *etc*, and thus can be characterized by different characterization techniques such as pump–probe magneto Kerr and Faraday signals, transient hysteresis loops for each time delay $\Delta t$ between the pump and probe laser.

Meanwhile, the flourishing of theoretical approaches, especially real-time *ab initio* methods, has been shown to contribute significantly to understanding the interactions between charge, lattice (or phonons), and spin. For example, Chen et al. studied ultrafast demagnetization in Ni using real-time time-dependent density functional theory (rt-TDDFT) calculations. Such a theoretical framework allows distinguishing the angular momentum transfer between photons, spins, and electron orbitals during the demagnetization process [23]. As Fig. 1b shows, the spin–orbit coupling effect is indispensable for the demagnetization while the spin Zeeman effect is negligible. More importantly, when turning off the lattice degree of freedom, *i.e.* fixing atoms in the simulation, there is a noticeable decrease in the demagnetization effect, highlighting that phonons play a nontrivial role in the angular momentum transfer. A similar message can be obtained from calculations on a two-atom Ni dimer, showing a clear exchange of angular momentum $L$ between electrons and ions on a sub-femtosecond timescale, shown in Fig. 1c.

The great advantage of temporal resolution on the order of femtoseconds to picoseconds lies in its correspondence to the crucial intrinsic magnetic energy scales (*e.g.*, magnetic anisotropy, spin–orbit coupling, exchange interactions, *etc.*), and interaction strengths between different degrees of freedom (Fig. 1a). In two-dimensional magnetic materials, such measurements serve as a unique approach that allows one to disentangle dynamics of various quasi-particles under nonequilibrium conditions [24]. On the other hand, two-dimensional materials with unique responses to external stimuli (gating, strain, *etc.*) provide unprecedented opportunities to study light-induced novel physical phenomena and to realize all-optical control [10,25–27]. It has been shown that various properties can be manipulated by light, such as lattice distortions [28,29], topological phase transitions [30,31], light-induced superconductivity [32–34]. Microscopically, photoexcitation can modify the potential energy surface landscape or the interaction strength between different degrees of freedom such as charge, lattice, and spin. Given their intrinsic lifetimes, optical excitation has the potential to manipulate materials' properties on an ultrafast timescale. Moreover, it does not rely on other external fields, such as strain fields, and has the advantages of reversibility, versatility, and high tunability.

A plethora of transitions or dynamics can be realized by further altering the frequency or fluence of the pump light. Phenomenologically, this can be understood from a simplified free energy landscape schematically shown in Fig. 2a. In the weak excitation regime, the system is driven not too far away from equilibrium and the induced variation can be treated as linear. The recovery process encodes information of various collective modes, thus allowing disentangling of the individual degree of freedom such as electrons, spins, and phonons. For example, Hu et al. demonstrated that the photoexcited carriers in graphene provide
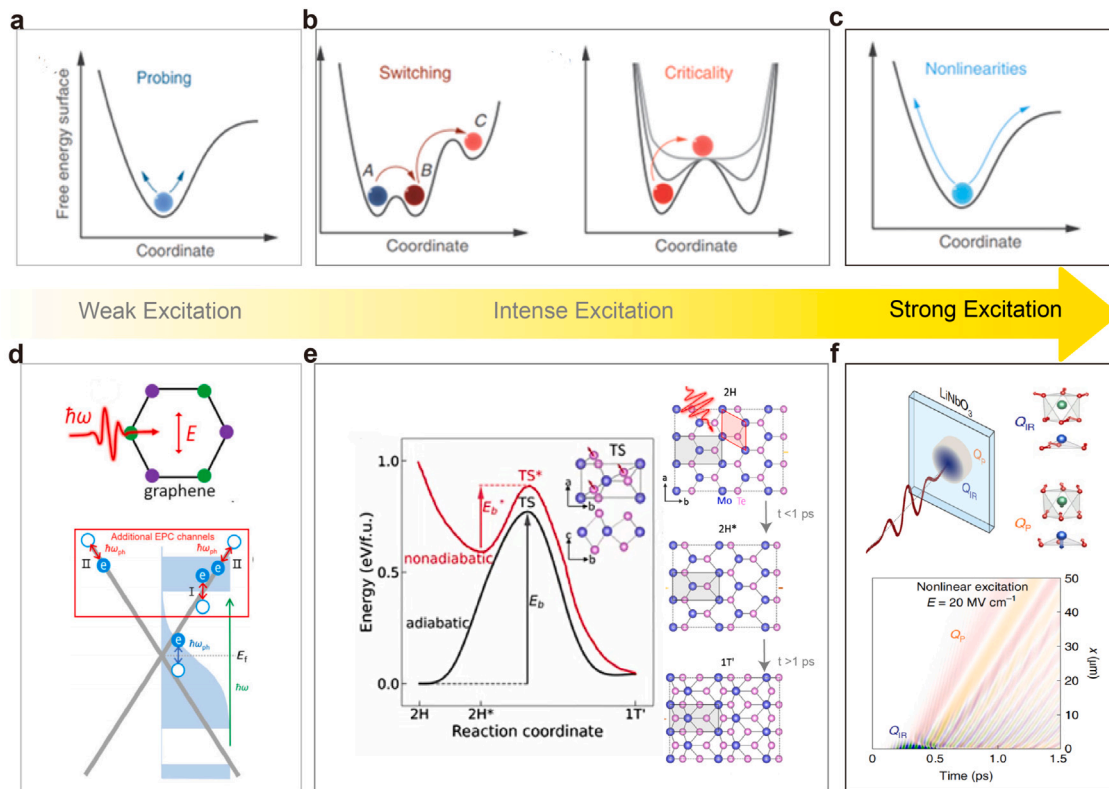
**Fig. 2.** Diagrams and examples of nonthermal pathways induced by optical excitation. (a) The weak excitation regime allowing effective probing of ultrafast quasiparticle dynamics. (b) The intense excitation regime where nonequilibrium switching and quantum criticality could be achieved due to large modification of the potential energy surface landscape. (c) The strong excitation regime where the nonlinear effects become non-negligible. (a–c) are reproduced from Ref. [35]. (d) Diagram showing additional electron–phonon scattering channels from nonequilibrium charge carriers in photoexcited graphene, reproduced from [36]. (e) Optical control of multistage phase transition *via* phonon coupling in monolayer MoTe$_2$, highlighting an intermediate 2H* structure, reproduced from [37]. (f) Nonlinear coupling between the photoexcited phonon modes $Q_{IR}$ and a propagating polariton mode $Q_P$ in bulk LiNbO$_3$, reproduced from [38].

additional channels for scattering with phonons due to their nonequilibrium distribution, which results in enhanced electron–phonon coupling [36]. As the intensity of laser excitation increases, ultrafast modifications of the transient free energy landscape can happen, shown in Fig. 1b. Such modifications could further induce phase transitions to metastable or nonequilibrium states and enable the study of nonthermal critical behaviors such as topological phase transition [29,30,39,40], light-induced superconductivity [32–34], *etc.* As an example, Guan et al. unraveled an intermediate structure 2H* during the light-driven phase transition from 2H to 1T′ in MoTe$_2$ monolayer, assisted by an unexpected phonon excitation and its coupling to the electronic states [37]. The excited phonon modes are determined by the photon energy and intensity of the laser pulse, indicating the system can be driven to a metastable and nonequilibrium state under intense excitation.

In addition to non-magnetic materials, more attention has been attracted to the investigations of dynamical manipulations in magnetic materials with the development of time-resolved spectroscopy such as pump–probe magneto-optics, time-resolved second-harmonic generation (SHG), two-photon photoemission, *etc.* Since magnetization is sensitive to electron excitation as well as lattice vibrations, nonlinear interactions are usually involved. In practice, this can take place via the intense light that drives the system far from equilibrium, where nonlinear couplings play an important role in dynamically modifying the coupling strength at high orders. Therefore, optical control of spins provides another strategy to investigate emergent phenomena from higher-order interactions, such as using nonlinear phonons under strong excitation to induce novel physical phenomena that are difficult to access by static approaches [11,41–44]. A very recent work from Henstridge et al. showed that the ferroelectric polarization reversal can be induced by the anharmonic coupling between the high-amplitude light-driven phonon modes in ferroelectric LiNbO$_3$ [38]. There, phonon–phonon interactions and/or other phonon-related nonlinearities play a crucial role in the strongly distorted crystal lattices. Taking together, the free energy landscapes in the three regimes mentioned above can in theory be tuned by varying the intensity of the laser pulse, which also indicates the versatility of all-light control.

Given the scientific significance and potential technological application, in this minireview, we discuss ultrafast all-optical control of magnetization dynamics in a variety of magnetic systems. First, we try to understand its physical origin from the perspective of theoretical models and quantum mechanics. We focus on the different roles played by each degree of freedom and the resulting novel physical phenomena that can arise on an ultrafast timescale (Section 2). We then discuss ultrafast dynamics in four exciting
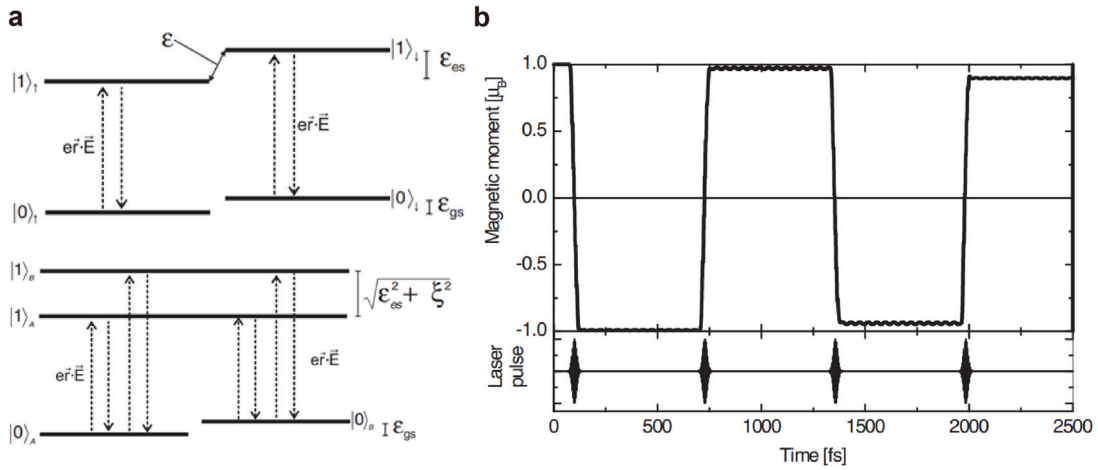
**Fig. 3.** The generic model for ultrafast photoinduced spin dynamics. (a) Illustration of energy levels without (upper panel) and with (lower panel) spin–orbit coupling. (b) Theoretical predictions on the all-optical control of magnetization switching in NiO(001) surface on the timescale of picoseconds. (a) and (b) are reproduced from Ref. [45] and Ref. [46], respectively.

aspects, *e.g.* photoinduced demagnetization, magnetization reversals, precessions, and magnetic phase transition, according to the characteristics of the dynamical processes (Section 3). In particular, for the latter two aspects, we review some very recent work on coherent-phonon-driven ultrafast magnetization precession and an antiferromagnetic to the ferromagnetic phase transition. These works provide direct evidence for manipulating spins via the lattice degree of freedom, and demonstrate the power of all-optical control which can be enlarged by the development and application of full-spectrum light sources. Our review shows that all-optical control has the potential to achieve ultrafast dynamical manipulation without relying on other external fields, which is of both fundamental scientific significance and practical value.

### 1.2. Ultrafast all-optical control of magnetization dynamics from a simplified analytical model

While the earliest all-optical control was mainly applied to the nonmagnetic semiconductors and metals [36,37,47–50], the study of all-optical control of magnetic materials did not start to attract attention until 1996, when an ultrafast demagnetization was observed in the ferromagnetic metal nickel by the pump–probe technique [12]. The idea of all-optical control of magnetization without other external fields has been explored extensively ever since, with the leaping development of ultrafast experimental methods.

Hübner et al. proposed a theoretical model on light-induced spin dynamics [45,46,51,52], which serves as the theoretical base for many recent works. There, the generic model of the photoinduced spin dynamics can be described by a four-energy-level system shown in Fig. 3a [45]. This effect can be briefly characterized by considering the spin splitting in the ground (excited) state with the energy of $\varepsilon_{gs}$ ($\varepsilon_{es}$), and the spin–orbit coupling interaction with a characteristic energy $\xi$. Using the pure spin states as the basis, the Hamiltonian of the four-level model system can be written as the following

$$H_0 = \begin{pmatrix} E_0 & 0 & 0 & 0 \\ 0 & E_0 + \varepsilon_{gs} & 0 & 0 \\ 0 & 0 & E_1 & \frac{\xi}{2} \\ 0 & 0 & \frac{\xi}{2} & E_1 + \varepsilon_{es} \end{pmatrix}.$$

(1)

The eigenvalues can be easily obtained by diagonalizing the Hamiltonian:

$$\varepsilon_{0\uparrow} = E_0$$
$$\varepsilon_{0\downarrow} = E_0 + \varepsilon_{gs}$$
$$\varepsilon_{1A} = E_1 + \frac{\varepsilon_{es}}{2} - \frac{1}{2}\sqrt{\varepsilon_{es}^2 + \xi^2}$$
$$\varepsilon_{1B} = E_1 + \frac{\varepsilon_{es}}{2} + \frac{1}{2}\sqrt{\varepsilon_{es}^2 + \xi^2}.$$

(2)

In the absence of the spin–orbit coupling interactions, *i.e.* $\xi = 0$, there is no coupling between different spin states and thus no spin dynamics occur. However, with a finite spin–orbit coupling strength $\xi = 0.1$ eV and taking $\varepsilon_{gs} = 0$, the spin switching can take place. By writing the system Hamiltonian in the form of $\hat{H}(\mathbf{r}, t) = \hat{H}_0(\mathbf{r}) + \hat{V}(\mathbf{r}, t)$ that consists of the time-independent part $\hat{H}_0(\mathbf{r})$ and the time-dependent part $\hat{V}(\mathbf{r}, t)$, the evolution of the eigenvalues can be obtained with the time-dependent light-driven external potential. The part of the time-independent Hamiltonian ($\hat{H}_0(\mathbf{r})$) is shown as Eq. (1), which represents the solution of the
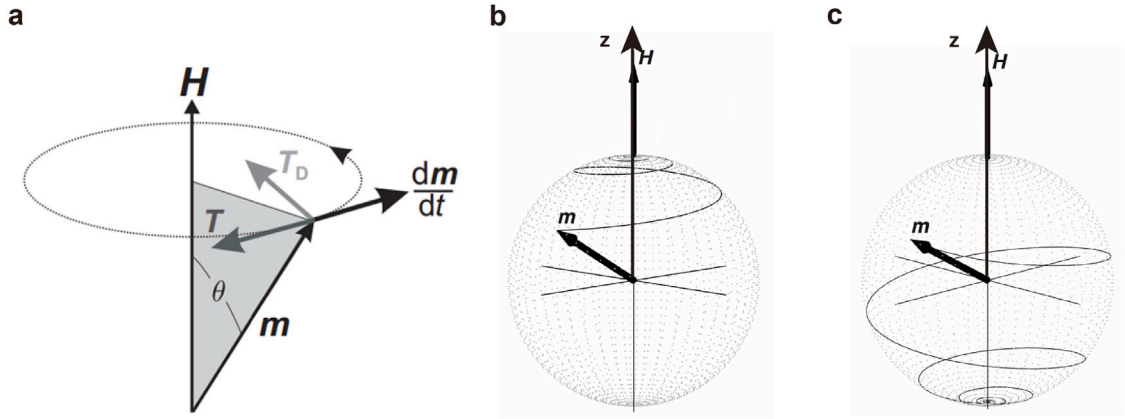
**Fig. 4.** A classical description of the precession motion of a magnetic moment. (a) The motion of the magnetic moment $m$ under the magnetic field $H$. At an angle of $\theta$, $m$ experiences a precessional torque $T$ and a damping torque $T_D$ that drives $m$ moving toward $H$. (b–c) Precessional motion of the magnetic moment $m$ along $z$ ($-z$) direction with a positive (negative) damping parameter $\alpha = 0.15$ ($\alpha = -0.15$), reproduced after Ref. [24].

electronic structure of the system of interest. And the other part $\hat{V}(\mathbf{r}, t)$ represents the interaction between the electronic system and the laser field. With the electric dipole approximation, the laser field induced by a periodically applied pulse can be described as $E(t) = E_0 \exp\left[-\left(\frac{t}{\tau}\right)^2 - i\omega_0 t\right]$. Using the surface gap state of ferromagnetic NiO(001) with proper discrete energy levels as an example, this work for the first time theoretically demonstrated all-optical spin switching on the subpicosecond timescale, as shown in Fig. 3b [46].

We note that, this analytical four-level model proposed by Hübner et al. is greatly simplified, yet it is the fundamental framework that encapsulates the essence of spin–orbit coupling interaction in the observed ultrafast spin dynamics. We acknowledge that this four-level Hamiltonian could not accurately depict the real magnetic system. For example, the phonon degree of freedom is totally absent in this model, which has been shown recently to be quite important and thus needs further investigation.

## 2. Theoretical approaches for ultrafast magnetization dynamics

### 2.1. The Landau-Lifshitz-Gilbert equation

We start from the classical description of the Landau–Lifshitz (abbreviated as LL equation in the following) equation traditionally used in the framework of classical mechanics. Under a magnetic field $H$, the torque $T$ that the magnetic moment $m$ experiences is

$$T = m \times H. \tag{3}$$

According to Newton's equation of motion $dL/dt = T$, Eq. (3) can be written as

$$\frac{dL}{dt} = T = m \times H. \tag{4}$$

The magnetic moment $m$ and the angular momentum $L$ can be connected through the gyromagnetic ratio $\gamma = \frac{qg\mu_0}{2m_e}$, i.e.

$$m = \gamma L, \tag{5}$$

where $\mu_0$, $g$, $m_e$, and $q$ denote the magnetic permeability of the vacuum, the Landau factor, the mass and charge of the electron, respectively.

Therefore, the motion of the magnetic moment $m$ in the magnetic field $H$ satisfies

$$\frac{dm}{dt} = \gamma[m \times H] = \gamma T. \tag{6}$$

At this point, the magnetic moment $m$ satisfies Lamor's precession motion in the magnetic field $H$. If there is only the precession term $T$, the magnetic moment $m$ precesses with respect to the direction of the magnetic field $H$. However, the magnetic moment will eventually align with the direction of the magnetic field, so an additional damping term $T_D$ must be introduced, which is perpendicular to the precession term $T$ and the magnetic moment $m$. It can be expressed as,

$$T_D = C\left[m \times \frac{dm}{dt}\right]. \tag{7}$$

The scaling factor $C = \frac{\alpha\gamma}{m}$ is similar to the coefficient of friction in the linear motion, where $\alpha$ denotes the damping factor implying an unspecified dissipation phenomenon. This classical description is schematically shown in Fig. 4a. It is thus obvious that

the positive values of $C(\alpha)$ cause the magnetic moment $\boldsymbol{m}$ to rotate towards the direction of $\boldsymbol{H}$, while negative $C(\alpha)$ causes the magnetic moment to be anti-aligned with $\boldsymbol{H}$, shown in Fig. 4b–c. The LL equation now reads

$$\frac{\mathrm{d}\boldsymbol{m}}{\mathrm{d}t} = \gamma[\boldsymbol{m} \times \boldsymbol{H}] + \frac{\alpha\gamma}{m}[\boldsymbol{m} \times (\boldsymbol{m} \times \boldsymbol{H})]. \tag{8}$$

Further, a modified version with a second-order damping term of the above LL equation, the Landau–Lifshitz–Gilbert (LLG) equation is often used, which reads

$$\left(1 + \alpha^2\right)\frac{\mathrm{d}\boldsymbol{m}}{\mathrm{d}t} = \gamma[\boldsymbol{m} \times \boldsymbol{H}] + \frac{\alpha\gamma}{m}[\boldsymbol{m} \times (\boldsymbol{m} \times \boldsymbol{H})]. \tag{9}$$

Here, when the damping term represented by the coefficient $\alpha$ is small, the second-order term can be neglected. Therefore, Eq. (9) can be written as

$$\frac{\mathrm{d}\boldsymbol{m}}{\mathrm{d}t} = \gamma[\boldsymbol{m} \times \boldsymbol{H}] + \frac{\alpha}{m}\left[\boldsymbol{m} \times \frac{\mathrm{d}\boldsymbol{m}}{\mathrm{d}t}\right], \tag{10}$$

which is equivalent to the LL equation (Eq. (8)).

Therefore, the LL or the LLG equation describes how $\boldsymbol{m}$ precesses with presence of a magnetic field $\boldsymbol{H}$. In combination with the three-temperature model (as will be discussed in greater detail in Section 3.1), the LL and LLG equations can describe the evolution of the direction of the magnetic moment $\boldsymbol{m}$ with time. However, it is worth mentioning that this treatment assumes that the magnitude of the magnetic moment $|\boldsymbol{m}|$ is constant, *i.e.* no longitudinal relaxation [53,54]. Besides, the phenomenological LLG equation cannot give a clear picture of the angular momentum transfer when spin is associated with the electronic structure.

### 2.2. Magnetization dynamics in the framework of time-dependent density functional theory

Different from the LL and LLG equations which only describe the evolution of the direction of the magnetic moment $\boldsymbol{m}$ in time, first-principles calculations can provide the time evolution of the magnetic moment, both its direction and magnitude, in the framework of the real-time time-dependent density functional theory (rt-TDDFT) [23,36,37,47–49,53,55,56].

The central idea is to self-consistently solve the Kohn–Sham equations describing the non-interacting single-particle system, assuming the total energy is a unique functional of the electron density following the Hohenberg–Kohn theorem. The time-dependent density functional theory has been developed following the Runge–Gross theorem [55,56], where the evolution of the electronic wavefunction can be described in the form of time-dependent Kohn–Sham equations:

$$i\hbar\frac{\partial}{\partial t}\psi_{n,\boldsymbol{k}}(\boldsymbol{r},t) = \hat{H}_{KS}\psi_{n,\boldsymbol{k}}(\boldsymbol{r},t). \tag{11}$$

The Hamiltonian $\hat{H}_{KS}$ can be written as

$$\hat{H}_{KS} = -\sum \frac{\hbar^2}{2m_i}\nabla_i^2 + V_{\mathrm{ION}} + V_{\mathrm{H}} + V_{\mathrm{XC}} + U_{\mathrm{ext}} + V_{\mathrm{soc}}, \tag{12}$$

where the terms in the equation represent, in order, the kinetic energy term of the electron $-\sum \frac{\hbar^2}{2m_i}\nabla_i^2$, the Coulomb potential generated by the nuclei $V_{\mathrm{ION}}$, the Hartree potential $V_{\mathrm{H}}$, the exchange–correlation potential $V_{XC}$, the external field $U_{\mathrm{ext}}$, and the spin–orbit coupling term $V_{\mathrm{soc}}$. Here the nuclei (with the index $l$) are treated classically with the average forces calculated according to the Ehrenfest theorem [47],

$$\boldsymbol{F}_l = -\int dr\psi_i^*(\boldsymbol{r},t)\nabla_l\hat{H}_{KS}(\boldsymbol{r},\boldsymbol{R},t)\psi_i(\boldsymbol{r},t). \tag{13}$$

To find solutions for the time-dependent magnetization dynamics, the time-dependent two-component Kohn–Sham spinors $\psi_{n,\boldsymbol{k}}(\boldsymbol{r},t)$ can be used to describe the electron spins, so that the local magnetic moment $\boldsymbol{m}(\boldsymbol{r},t)$ at the position of $\boldsymbol{r}$ at time $t$ can be expressed as [23,57]

$$\boldsymbol{m}(\boldsymbol{r},t) = \mu_B \sum_{n,\boldsymbol{k}} \psi_{n,\boldsymbol{k}}^\dagger(\boldsymbol{r},t) \cdot \hat{\sigma} \cdot \psi_{n,\boldsymbol{k}}(\boldsymbol{r},t), \tag{14}$$

with $\hat{\sigma}$ being the Pauli matrices and $n$ the band index. The total magnetization $M(t)$ at the moment $t$ can thus be calculated directly from the time-dependent Kohn–Sham spinors as

$$M(t) = \int \boldsymbol{m}(\boldsymbol{r},t)d\boldsymbol{r}. \tag{15}$$

*Ab initio* calculations based on TDDFT have been shown to be a powerful tool to theoretically address fundamental questions in ultrafast magnetization dynamics. In addition to the work mentioned in Section 1.1, studies on high harmonic generation [50], photoinduced demagnetization [23], magnetization reversal [46] *etc.*, have offered tremendous insights into the coupling dynamics between spins and other quasiparticles. This provides additional opportunities to understand the underlying mechanism for the magnetization dynamics experimentally observed, most time indirectly, with various ultrafast techniques, and make reliable predictions to harness the desired functionality of materials for technological applications.
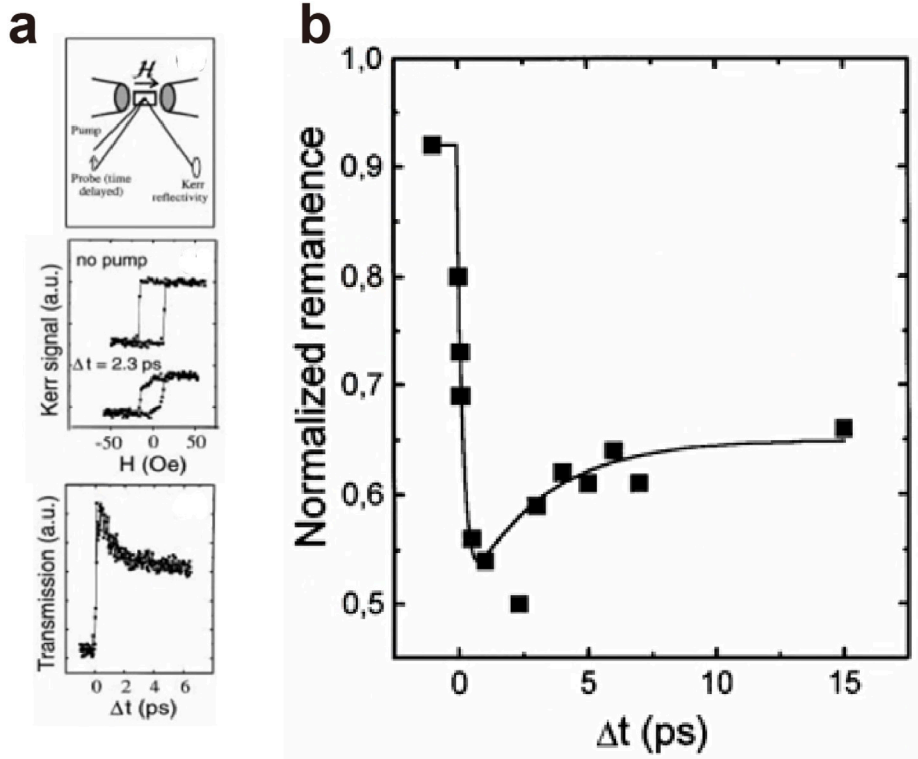
**Fig. 5.** Ultrafast demagnetization in Ni thin film. (a) The experimental pump–probe setup, highlighting the temporal change in the Kerr signal and transmission after the pump pulse. (b) Transient longitudinal magneto-optical Kerr signal observed in a 20 nm Ni thin film on $MgF_2$ after excited by a pump pulse with a fluence of 7 mJ/cm². The signal values are normalized to those measured without the pump light. (a) and (b) are reproduced from Ref. [12].

## 3. Emergent ultrafast manipulation of magnetization

### 3.1. Ultrafast light-induced demagnetization

The earliest study on light-induced demagnetization dates back to 1990 when Meier et al. first captured the time evolution of nonequilibrium magnetic states in ferromagnetic metallic gadolinium (Gd) on the femtosecond timescale by time-resolved spin-polarized photoemission spectroscopy (TRSPPS) [59]. A characteristic timescale of $100 \pm 80$ ps is determined for the heat transfer from the lattice system to the spin system, *i.e.* the spin–lattice relaxation time. Later, Hübner and Bennemann theoretically modeled the demagnetization time of Gd to be about 48 ps, which lies in the same range as the experiment [60]. In the same year, Beaurepaire et al. used the ultrafast optical and magneto-optical pump–probe techniques to study the relaxation of the electrons and spins in ferromagnetic metallic nickel (Ni) films by measuring the transient Kerr and transmission signal after a pump pulse, shown in Fig. 5a. Fig. 5b shows the normalized remanence from the magneto-optical Kerr signal, where they found that the magnetization decreases rapidly within the first picosecond and reaches the minimum within two picoseconds [12]. This study for the first time highlights the contributions of electron–spin interactions to the demagnetization dynamics on the picosecond timescale.

At that time, the theoretical understanding was mostly based on the three-temperature model (abbreviated as 3TM) [12,54,61]. There, spin, lattice, and electron charge are considered as three heat baths, with their corresponding temperature denoted by $T_s$, $T_l$, and $T_c$, respectively, as shown in Fig. 6a. The dynamics of the system can thus be described by three coupled differential equations as follows [1,12,53,58,62,63]

$$C_e\left(T_e\right)\frac{dT_e}{dt} = -G_{el}\left(T_e - T_l\right) - G_{es}\left(T_e - T_s\right) + P(t)$$

$$C_s\left(T_s\right)\frac{dT_s}{dt} = -G_{es}\left(T_s - T_e\right) - G_{sl}\left(T_s - T_l\right)$$

$$C_l\left(T_l\right)\frac{dT_l}{dt} = -G_{el}\left(T_l - T_e\right) - G_{sl}\left(T_l - T_s\right). \tag{16}$$

Here $C_e$, $C_l$, and $C_s$ denote the electron, lattice, and spin heat capacity, respectively. $G_{el}$, $G_{es}$, $G_{sl}$ are the electron–lattice, electron–spin, and spin–lattice coupling constants, which can be obtained from fitting the experimental data. Lastly, $P(t)$ refers to the radiation heating from the external laser field. After laser excitation, the energy of the pump laser is absorbed by electrons on the timescale of optical pulse duration. Afterward, the energy is transferred from the electron bath to the spin and lattice subsystems, where the
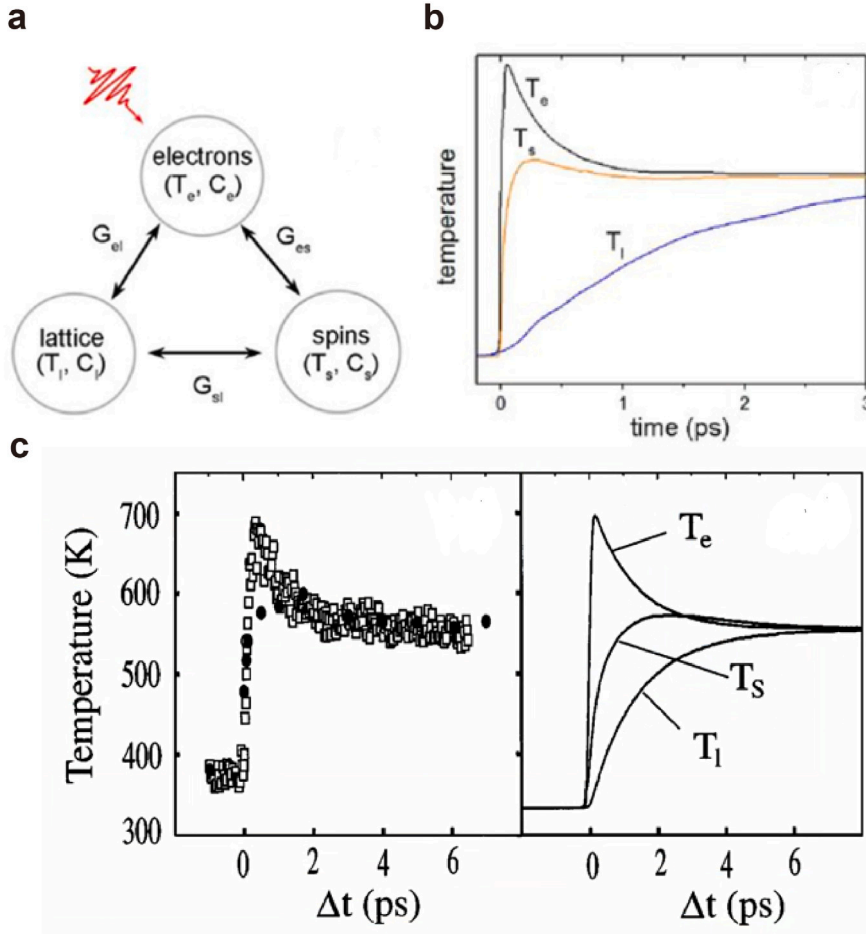
**Fig. 6.** The three temperature model and its time evolution. (a) Schematic diagram of the three-temperature model with relevant parameters explained in Eq. (16) in the main text. (b) Schematics of the temporal evolution of temperature in the three-temperature model. (c) Experimental spin temperature $T_s$ (in solid circle) and electron temperature $T_e$ (in blank square) (the left panel) and the estimated temperatures for the three heat baths (the right panel) in Co/garnet system. (a) and (b) are reproduced from Ref. [58] and (c) is reproduced from Ref. [12].

subsequent timescales depend on the strength of interactions among different degrees of freedom. Here, the values of $G_{el}$, $G_{es}$, and $G_{sl}$ characterize the strengths of electron–lattice, electron–spin, and spin–lattice interactions, respectively. The concept of temperature exchange is established through energy transfer *without* considering the angular momentum transfer. Yet, it describes the observed demagnetization dynamics in ferromagnetic materials (for example, Ni) in a quantitative way as Fig. 6b–c show and to some extent illustrates the role played by each degree of freedom from the dynamical perspective.

It is not surprising that there are still questions about the coupling mechanism, which are not fully explained by the three-temperature model and have motivated a great amount of work to further explore the underlying physics both theoretically and experimentally in a greater depth. As an example, Hohlfeld et al. first observed that the magnetic response is faster than the electron thermalization by pump–probe second-harmonic generation (SHG) in Ni, presumably due to the significant difference (about twice) in the lifetimes of the majority-spin and minority-spin of the excited electrons [14], similar to the mechanism proposed by Koopmans and Aeschlimann [53]. Meanwhile, Scholl et al. used time-dependent photoelectron spectroscopy with spin analysis and observed demagnetization on two different timescales. One is the fast demagnetization on the timescale of sub-picosecond, during which Stoner pairs are generated by the excited hot electrons from the electron–electron interactions, whereas the slower one is within a few hundred picoseconds, dominated by the spin–lattice relaxation [63].

Later, Zhang and Hübner argued that the three-temperature model is quasi-static and the concept of spin temperature itself is questionable due to the lack of well-defined spin quasiparticle statistics [51,64]. Therefore, they give a quantum description of ultrafast nonequilibrium charge and spin dynamics based on the exact diagonalization framework [65]. This theoretical approach is not based on the perturbation theory and is thus more suitable for characterizing dynamics far from equilibrium, which is usually the case under optical excitation. As mentioned in Section 1.2, the Hamiltonian $H = H_{\mathrm{sys}} + H_{\mathrm{ext}}$ consists of two parts: $H_{\mathrm{sys}}$ for the system and $H_{\mathrm{ext}}$ for the laser field which evolves in time. The Hamiltonian of the system corresponding to the demagnetization

upon laser excitation at the femtosecond scale is

$$H_{sys} = \sum_{i,j,k,l,\sigma,\sigma',\sigma'',\sigma'''} U_{i\sigma,j\sigma',k\sigma'',l\sigma'''} c_{i\sigma}^{\dagger} c_{j\sigma'}^{\dagger} c_{k\sigma''} c_{l\sigma'''} + \sum_{\nu,\sigma,K} \mathcal{E}_{\nu}(K) n_{\nu\sigma}(K) + H_{SOC}, \qquad (17)$$

where $U_{i\sigma,j\sigma',k\sigma'',l\sigma'''}$ is the on-site electron interaction, which can be described by the three parameters, the Coulomb repulsive potential $U$, the exchange interaction $J$, and the exchange anisotropy $\Delta J$. $\mathcal{E}_{\nu}(K)$ represents the spin-independent band structure. $n_{\nu\sigma}(K)$ is the particle number operator of band $n$ in reciprocal space. $H_{SOC}$ represents the term of spin–orbit coupling (SOC) interaction. For the case of ferromagnetic metal Ni, the three generic values obtained by fitting the experimental spectroscopic data are 12 eV, 0.99 eV, and 0.12 eV for on-site interaction $U$, the exchange interaction $J$, and the exchange anisotropy $\Delta J$, respectively.

Although the proposed Hamiltonian is initially applied to Ni, it has universal applicability in revealing the general internal and external factors related to the spin dynamics in ferromagnetic materials on the femtosecond scale. In addition to the five internal factors mentioned above ($U$, $J$, $\Delta J$, $H_{SOC}$, $\mathcal{E}_{\nu}$), this Hamiltonian also takes into account the external factors, including the photon frequency of the pump and probe light, the fluence and duration of the pump laser, and the measurement errors of different instruments, *etc.* Following this framework, it has now been widely accepted that the ultrafast spin dynamics could typically be divided into four stages based on the timescales: (1) electron thermal equilibrium (on the timescale of 1 fs), (2) electron–spin relaxation (on the timescale of a few femtoseconds), (3) electron–lattice relaxation (on the timescale of 1 ps), and (4) spin–lattice relaxation (on the timescale about 100 ps) [51,52,64].

Meanwhile, Koopmans et al. attempted to describe the microscopic mechanism of the femtosecond demagnetization phenomenon based on the Landau–Lifshitz–Gilbert (LLG) equation. Their model considers that the relaxation between the spin, lattice, and electron in a similar manner to a macroscopic magnetization precession of the magnetic moment with the presence of an effective magnetic field. The authors demonstrated the spin dynamics in Ni and Co in the framework of the LLG equation, without taking into account the thermal fluctuation effect. They also discussed the significance of the LLG damping term, arguing that the essential characteristic demagnetization time is related to impurity-induced spin scattering [45,49].

This work further indicates that the demagnetization physically originates from the interactions between the electron, phonon, and spin degrees of freedom. Although the role of phonons has been addressed in a subsequent work [23], in-depth exploration is still lacking. How the phonon degree of freedom comes into play is of great importance for the optical manipulation of magnetic materials as selectively driving a coherent phonon becomes accessible in experiments, and great efforts are still needed to improve our understanding [66].

### 3.2. Ultrafast magnetization reversal

Magnetization reversal has long been recognized as a fundamentally interesting issue with great potential for the future development of magnetic recording and information processing. For example, in the context of thermomagnetic writing, it was shown that information can be recorded *via* magnetization reversal induced by ultrafast heating of a magnetic medium of GdFeCo in the presence of an external field [62,67]. Further, a femtosecond laser can act as irradiation to the magnetic material and improve the ultimate writing speed. Although it is intuitive from the LLG equation that the appearance of a negative damping term may correspond to the appearance of the magnetization reversal (Fig. 4c) [24], the complete understanding of magnetization reversal is still under pursuit even until now.

As Fig. 7a shown, Vahaplar et al. in 2009 observed the magnetization reversal of the magnetic domain in the ferromagnetic alloy $Gd_{24}Fe_{66.5}Co_{9.5}$ on the timescale of tens of picoseconds induced by circularly polarized light, which the authors attributed to the heating of the magnetic sample by femtosecond laser pulses, or the energy transfer from the magnetic sample to the spin bath. However, the final magnetic order is determined by both the initial magnetic order and the helicity of the circularly polarized light, whose role was not fully understood. Later in 2012, Ostler et al. demonstrated from a model point of view that the two unequal magnetic sublattices in the GdFeCo alloy are necessary for magnetization reversal. The "lattice-electron" two-temperature model implies a rapid temperature increase in the electron heat bath caused by the femtosecond laser, which is transferred to the lattice heat bath through the electron–phonon interaction. The magnetization reversal then results from the coupling and energy transfer between the phonon and the spin system. More importantly, they gave experimental evidence that the magnetization reversal can be induced by a laser with sufficient intensity, independent of the helicity of the femtosecond laser pulse, as shown in Fig. 7(b) [67]. It can be seen that under weak excitation the magnetic reversal is determined by the helicity of the light; under intense excitation, the magnetic reversal phenomenon does not depend on the helicity of the light. In addition, Xu et al. argued the role of hot-electron pulses could be similar to the ultrafast magnetization reversal in the multilayer structure: Glass/Ta (3 nm)/Pt (5 nm)/Cu (80 nm)/$Gd_x$[FeCo]$_{1-x}$ (5 nm)/Ta (5 nm) (Fig. 7) induced by femtosecond light pulses. There, the same magnetization reversal effect can take place when pumping the sample on the buffer layer on the Pt-side using femtosecond laser pulses, although irradiating the buffer layer takes about four times the intensity of that on the Ta-side. Therefore, they suggest that the magnetization reversal by femtosecond laser pulses is essentially the hot electron effect of the laser through the medium. The effect of femtosecond laser pulses is considered to induce a rapid increase in the temperature of the electron heat bath, which transfers energy to the spin system, thus causing the reversal of magnetization. The role of phonons was not considered in this work [69].

In addition to the above-mentioned ferromagnetic alloy GdFeCo or TbFeCo [71] containing $4d$ rare earth elements and $3d$ transition metal elements, magnetization reversal was achieved very recently using circularly polarized light in a three-layer two-dimensional van der Waals ferromagnet $CrI_3$ [72]. The phase diagram of magnetization reversal in the three-layer $CrI_3$ is related to the helicity of circularly polarized light, the photon energy, and the pump fluence. Besides, different photon energies are needed
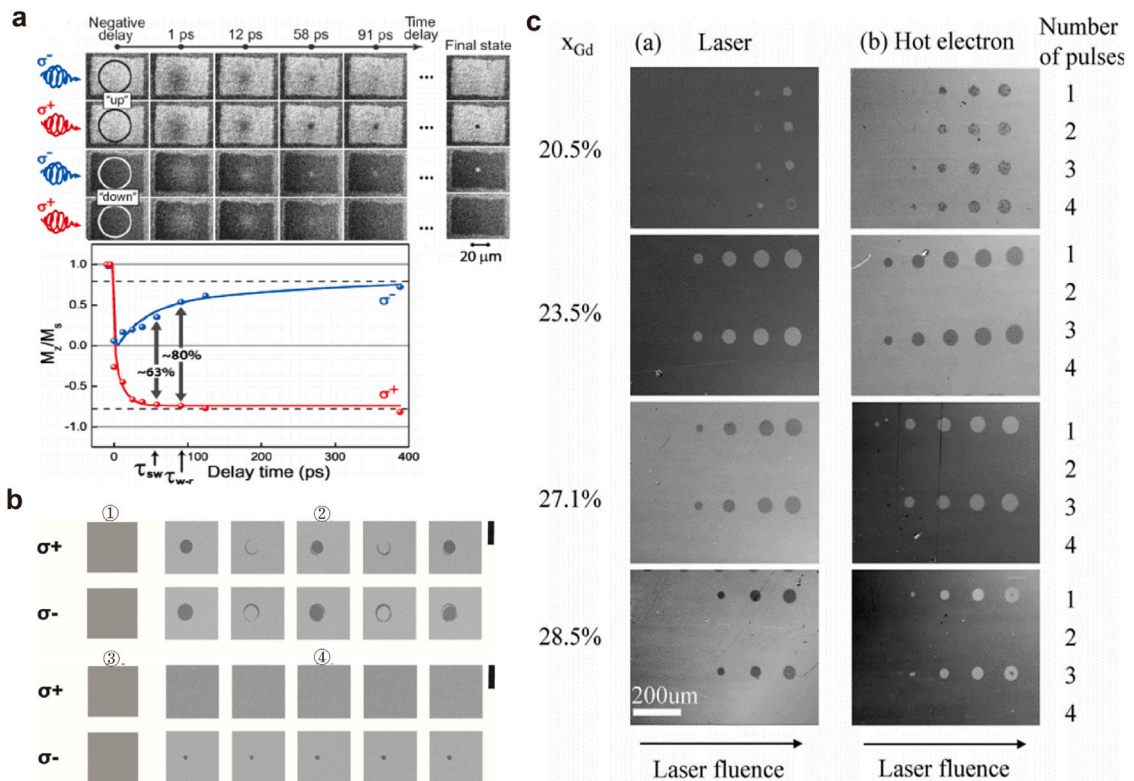
**Fig. 7.** Light induced magnetization reversal in magnetic alloys. (a) Images of the magnetic domain of $Gd_{24}Fe_{66.5}Co_{9.5}$ alloy, as well as the total magnetization along $z$ at different time after pumped by the right-handed ($\sigma^+$) and left-handed ($\sigma^-$) circularly polarized pulses at room temperature. (b) The magneto-optical images of $Gd_{24}Fe_{66.5}Co_{9.5}$ films obtained after the number N of 100 fs right-handed ($\sigma^+$) and left-handed ($\sigma^-$) circularly polarized laser pulse. ① and ③ show the initial magnetic states. ② shows the film after excitation with N (N=1,2...5) circularly polarized laser pulses with a large fluence of 2.30 mJ/cm$^2$. ④ shows the film after excitation with N (N=1,2...5) circularly polarized pulses with a small fluence of 2.25 mJ/cm$^2$. The scale bar indicates a length of 20 μm. (c) The magneto-optical Kerr images of the GdFeCo alloy at four different pump fluences (ranging from 0.75 to 3.5 mJ/cm$^2$) in the direct femtosecond laser excitation regime and the indirect hot electron excitation regime (from 4 to 12.25 mJ/cm$^2$), showing similar reversal effect can also be induced from both mechanisms. (a), (b), and (c) are reproduced from Ref. [68] and Ref. [67] and Ref. [69], respectively.

for right-handed and left-handed pulses, indicating that the ultrafast magnetization reversal in CrI$_3$ is related to specific excitation levels and angular momentum transfer between spins of different electronic states. Although the spin angular momentum transfer mechanism provides a better understanding of the interactions involved with photons, electrons, and spins, the role of phonons has rarely been reported in these studies. To our best knowledge, the most widely accepted mechanism for laser-induced magnetization reversal is *via* electron–phonon mediated spin-flip scattering proposed by Koopmans et al. It demonstrates the role of phonons based on the three-temperature model (3TM), but does not provide any detailed insight into microscopic origin of the dynamic processes involved [73]. Therefore, more attention needs to be paid both experimentally and theoretically to the accompanying phonon dynamics to better understand the underlying mechanism in all-optical control of magnetization dynamics.

### 3.3. Ultrafast magnetization precession from coherent phonons

Laser-induced coherent magnetization precession in a variety of quantum materials manifests itself in a coupled dynamics between magnetic moment and angular momentum [62]. Systems with magnetization precessions are regarded as a unique playground to study the evolution of angular momentum in the optical control of magnetization considering the angular momentum conservation. As a result, tremendous efforts have been devoted to investigating the ultrafast precessions in different systems [74–77]. Magnon, a quantized spin wave reflecting the collective excitation of electron spins, is a strong indication of coherent spin precession and can be observed by transient birefringence measurement in ultrafast optical experiments.

Garnets such as DyFeO$_3$ [42], ErFeO$_3$ [78], *etc.* are of great value to realize the magnetization precession due to a minimal absorption at the excitation wavelength of 800 nm and a different response to the pump pulse polarization. Therefore, the precession of magnetic moment with the opposite phase in DyFeO$_3$ thin films can be triggered by the left- and right-handed circularly polarized laser pulses incident along the $z$-axis imposed to an in-plane applied magnetic field [78].

Furthermore, the nonlinear effects of light on the magnetization allow for ultrafast coherent control of spin precession. For example, Nova et al. observed the excitation of magnetization precession *via* the nonlinear phononics in the rare-earth orthoferrite
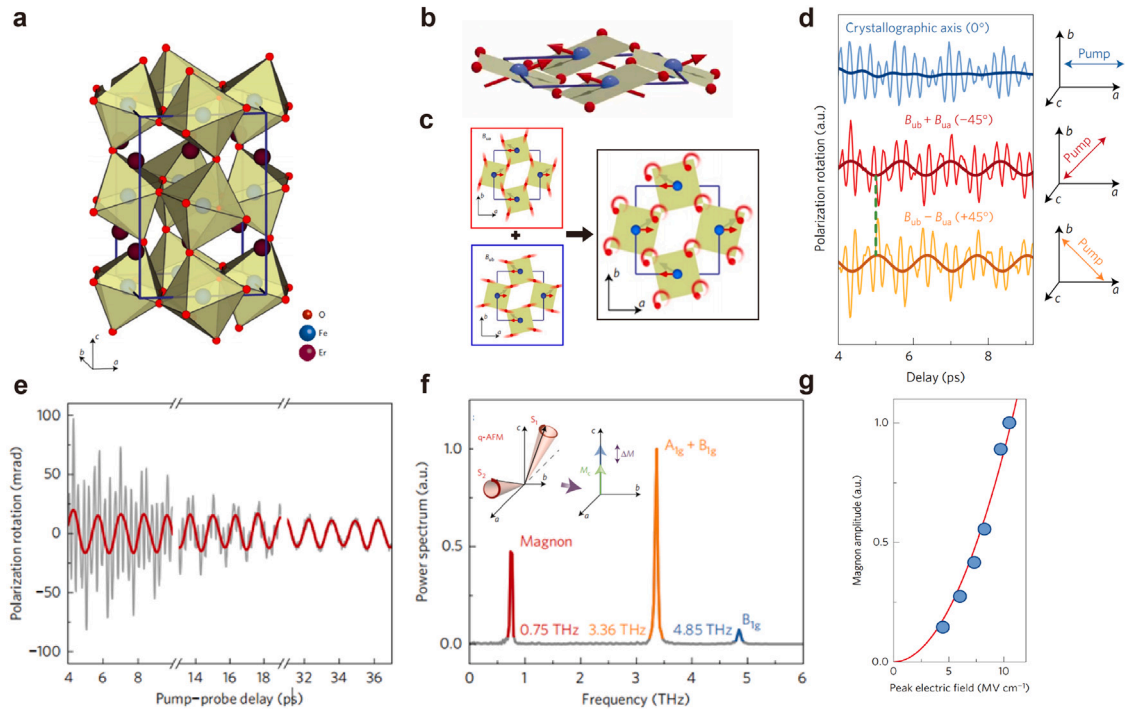
**Fig. 8.** Ultrafast magnetization precession in ErFeO$_3$. (a) Crystal structure of ErFeO$_3$, highlighting the orthorhombically distorted perovskite structure. (b) Magnetic order in ground state where the spins of iron ion align antiferromagnetically along $a$ axis but with a canted angle. (c) Atomic motions for the photoinduced infrared-active phonon modes B$_{ua}$ and B$_{ub}$. The motion of the individual ions produced by the superposition exhibits a circular motion with elliptical polarization. (d) Coherent magnon oscillations at different pump pulse polarization. (e) Transient birefringence measurement at 100 K. The excitation of spin precession, where the multi-component fast oscillations (in gray line) can be filtered out by a low-pass filter (1.5 THz cutoff) to reveal the slow oscillations associated with magnon (in red). (f) FFT results of the oscillations. The polarization of the probe oscillates in time, which includes the slow component (at 0.75 THz) and fast components (at 3.36 THz and 4.85 THz, respectively). The magnetic response indicates a quasi-antiferromagnetic (q-AFM) magnon (in red peak), associated with the superposition peak of A$_{1g}$+B$_{1g}$ phonons (in orange peak) and B$_{1g}$ phonons (in blue peak). The insets show a cartoon plot of spin motions (S$_1$ and S$_2$) in the q-AFM mode with the magnetization variation in $c$ axis. (g) Dependence of the magnon amplitude on the electric field of the pump laser. (a)–(g) are reproduced from Ref. [42]. (For interpretation of the references to color in this figure legend, the reader is referred to the web version of this article.)

ErFeO$_3$ [42]. This antiferromagnetic insulator crystallizes in an orthorhombically distorted perovskite structure with canted spins, as shown in Fig. 8a. The infrared active in-plane $B_{ua}$ and $B_{ub}$ phonon modes can be driven by laser excitation at 20 THz frequency and their superposition can induce the generation of circularly polarized phonon modes. With the light polarization at an angle from $a$-axis of +45° or −45°, the two modes with an opposite nonzero relative phase form opposite circular polarized atomic motion, indicated in Fig. 8b-d. The effect of nonlinear phonon modes mimics the application of a magnetic field and thus contributes to the generation of magnons. The induced magnons at a frequency of 7.5 THz feature a quasi-antiferromagnetic magnetic mode (q-AFM) with the modulation of the magnetic moment along the $c$-axis, shown in Fig. 8f. Moreover, the phase of the magnetization oscillations is proved to have a strong dependence on the relative phase of the two driven phonons while no dependence on initial magnetic orders. The ultrafast magnetization precessions characterized by magnons are shown to be related to temperature, frequency, phonon amplitude (Fig. 8g), as well as the polarization of the laser pulses (Fig. 8e) [42].

Realizing all-optical quantum control of magnetization precessions is extremely appealing, yet such a process has still been quite rare up to now. A better understanding of the underlying mechanism is greatly demanded. Specifically, the role of phonon coupling and their angular momentum exchange with spins deserve more consideration and in-depth exploration.

### 3.4. Nonlinear phonon induced AFM to FM magnetic phase transitions

Phase transition between magnetic states has been a well-sought-after physical phenomenon relevant to enormous practical applications and fundamental theoretical questions. Particularly, magnetic materials that undergo a coupled structural transition offer new insight into the interplay between multiple degrees of freedom. Different from the conventional way of inducing magnetic phase transitions using external magnetic field, pressure, temperature, *etc*, the experimental development of ultrafast all-optical quantum control has provided new means to realize magnetic phase transition in the sub-picosecond time regime.

A great amount of work has investigated ultrafast phase transitions in recent years [79–84]. Early in 2004, Ju et al. observed the first-order antiferromagnetic-to-ferromagnetic phase transition accompanying a lattice expansion in thin metallic FeRh films on
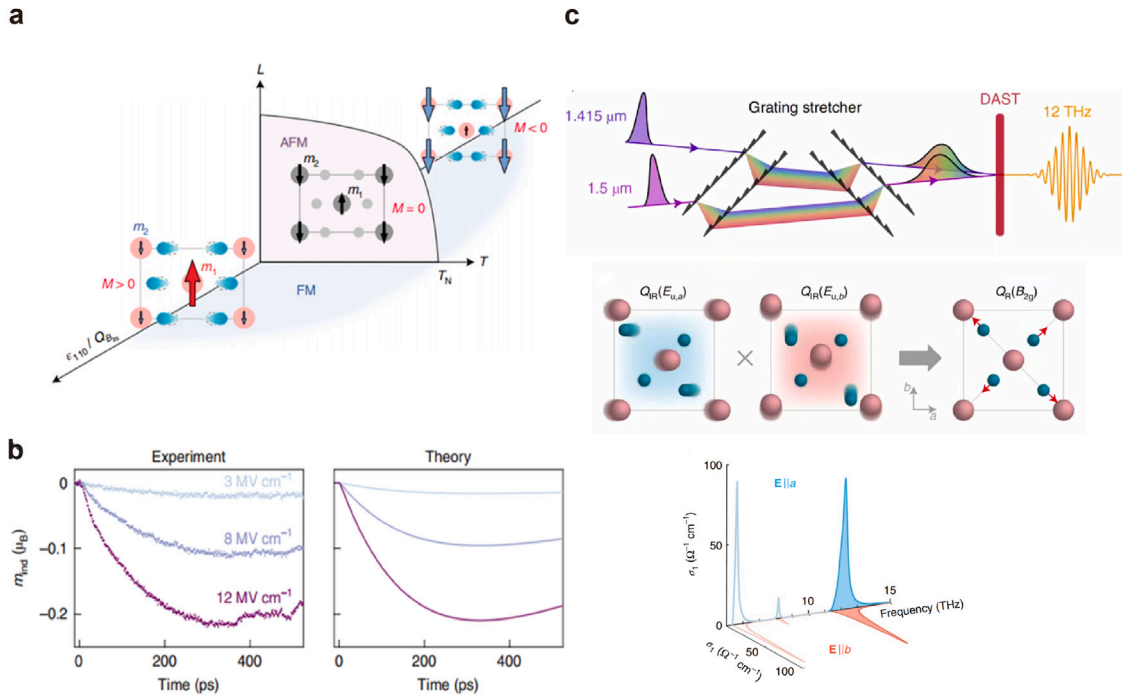
**Fig. 9.** Light induced magnetic phase transition in CoF$_2$. (a) Spin configurations of CoF$_2$. Pristine bulk CoF$_2$ is antiferromagnetic below the Néel temperature T$_N$. Upon distortion, the magnetic moments on the Co sites ($m_1$ and $m_2$) cannot be canceled, inducing the generation of ferromagnetic order and non-zero magnetic moments ($M$). The lattice distortion (described in the $a-c$ plane) can be generated by either a uniaxial strain along the crystallographic [110] direction or by atomic displacement along the B$_{2g}$ Raman phonon mode. (b) Comparison of theoretical and experimental results on the ultrafast magnetization dynamics of CoF$_2$ after light excitation with different optical fluences, illustrating a photoinduced net magnetization and its tunability. (c) Light-induced degenerate infrared phonons. The nonlinear coupling between the two orthogonal, degenerate infrared active E$_u$ phonons induces a symmetry-breaking B$_{2g}$ Raman phonon mode and as a result displaces the lattice. The lower panel shows the optical conductivity of CoF$_2$ at 6 K along the two orthogonal in-plane crystal axes ($a$ and $b$ in blue and red, respectively) with three (E$_u$ symmetry) IR modes at 6, 8, and 12 THz. By pumping the modes at 12 THz (peaks in solid shading), a B$_{2g}$ Raman mode can be excited. All figures are reproduced with permission from Ref. [70]. (For interpretation of the references to color in this figure legend, the reader is referred to the web version of this article.)

the sub-picosecond timescale. The underlying mechanism is considered to be strong exchange interactions from the increased spin temperature induced by the laser. However, it has not provided enough evidence for the microscopic origin of the complex interplay between lattice, electron, and spin [79–81].

In particular, Disa et al. recently proposed a phase transition from antiferromagnetic to ferromagnetic state in bulk anti-ferromagnet CoF$_2$ and showed it can be realized by the coherent light-induced nonlinear phonons [70]. As Fig. 9c shown, two infrared active E$_u$ phonon modes can be induced directly by terahertz (THz) laser pulses, and their strong anharmonic coupling can introduce a Raman active B$_{2g}$ mode, resulting in a symmetry-breaking distortion of the lattice.

CoF$_2$ in its pristine state is a Néel-type antiferromagnet with Néel temperature T$_N$ = 39 K. Upon symmetry-breaking, the local magnetic moments on the two Co atoms are not fully canceled out, yielding a net magnetic moment of 0.2 $\mu_B$ per unit cell (shown in Fig. 9a), which is nearly three orders of magnitude larger than the magnetic moment induced by mechanical strain previously proposed by Radaelli et al. [85]. Furthermore, the net magnetization in CoF$_2$ can be manipulated by varying the fluence of the pump pulse, as shown in Fig. 9b, showing a strong tunability of all-optical control. Therefore, all-optical control of phonon-driven magnetic phase transitions offers a new mechanism to manipulate magnetism, and thus potentially advancing the study of out-of-equilibrium phase transition behaviors in magnetic materials.

Similar to the previous aspect, this case of ultrafast magnetic phase transition also highlights the significant role of phonons in ultrafast magnetization dynamics, especially the nonlinear coupling of phonon modes. The idea of ultrafast magnetization manipulation *via* phonons allows for further exploration of spin–phonon–electron–photon interactions and is likely to open up new avenues for the manipulation of high-speed and low-power spintronic devices.

## 4. Conclusions and outlook

After nearly three decades of development, the area of ultrafast all-optical control of magnetization dynamics is now an exciting and fast-growing research area in condensed matter physics. The purpose of this article is to briefly review various aspects on both theoretically proposed and experimentally observed ultrafast magnetization dynamics induced by optical excitation in magnetic materials, including ferromagnetic and antiferromagnetic metals, semiconductors, and alloys containing rare earth elements. These

studies show that femtosecond laser pulses are indeed one of the novel and effective ways to induce a wide range of magnetization dynamics, and all-optical controlled magnetic phenomena have great potential in inspiring next-generation device concepts. In addition, recent advances in accessing laser pulses with a wide range of frequency (from terahertz to X-ray), fluence (up to $10^{22}$ W/cm$^2$), and duration (down to the attosecond scale) provide great opportunities to study ultrafast magnetization dynamics as the coupling between different degrees of freedom features various characteristic timescales. We also attempt to understand the ultrafast all-optical control of magnetization dynamics by reviewing theoretical frameworks from the classical picture provided by the Landau–Lifshitz–Gilbert equation to the *ab initio* rt-TDDFT theory.

At this point, theoretical progress is unprecedentedly needed since there are still many open questions on how to identify the physical origins of ultrafast magnetization dynamics under optical excitation. The central challenge is to fully trace the fundamental role played by the interactions among the various degrees of freedom in quantum materials, especially those with nontrivial band topology, strong correlation, quantum criticality, *etc*. Future developments in ultrafast all-optical controlled magnetization dynamics will keep giving rise to interesting and far-reaching physical phenomena and may revolutionize the data storage and information processing technologies.

## Declaration of competing interest

The authors declare that they have no known competing financial interests or personal relationships that could have appeared to influence the work reported in this paper.

## Acknowledgments

## References

[1] C. Wang, Y. Liu, Nano Convergence 7 (1) (2020) 35.
[2] B. Huang, G. Clark, E. Navarro-Moratalla, D.R. Klein, R. Cheng, K.L. Seyler, D. Zhong, E. Schmidgall, M.A. McGuire, D.H. Cobden, W. Yao, D. Xiao, P. Jarillo-Herrero, X. Xu, Nature 546 (7657) (2017) 270–273.
[3] B. Huang, G. Clark, D.R. Klein, D. MacNeill, E. Navarro-Moratalla, K.L. Seyler, N. Wilson, M.A. McGuire, D.H. Cobden, D. Xiao, W. Yao, P. Jarillo-Herrero, X. Xu, Nature Nanotechnol. 13 (7) (2018) 544–548.
[4] T. Song, Z. Fei, M. Yankowitz, Z. Lin, Q. Jiang, K. Hwangbo, Q. Zhang, B. Sun, T. Taniguchi, K. Watanabe, M.A. McGuire, D. Graf, T. Cao, J.-H. Chu, D.H. Cobden, C.R. Dean, D. Xiao, X. Xu, Nature Mater. 18 (12) (2019) 1298–1302.
[5] S. Liu, X. Yuan, Y. Zou, Y. Sheng, C. Huang, E. Zhang, J. Ling, Y. Liu, W. Wang, C. Zhang, J. Zou, K. Wang, F. Xiu, Npj 2D Mater. Appl. 1 (1) (2017) 30.
[6] A. Bafekry, M. Faraji, S. Karbasizadeh, I.A. Sarsari, H.R. Jappor, M. Ghergherehchi, D. Gogova, Phys. Chem. Chem. Phys. 23 (42) (2021) 24336–24343.
[7] K.S. Burch, D. Mandrus, J.-G. Park, Nature 563 (7729) (2018) 47–52.
[8] X. Jiang, Q. Liu, J. Xing, N. Liu, Y. Guo, Z. Liu, J. Zhao, Appl. Phys. Rev. 8 (3) (2021) 031305.
[9] V.P. Ningrum, B. Liu, W. Wang, Y. Yin, Y. Cao, C. Zha, H. Xie, X. Jiang, Y. Sun, S. Qin, X. Chen, T. Qin, C. Zhu, L. Wang, W. Huang, Research 2020 (2020) 1–19.
[10] Y. Yao, X. Zhan, M.G. Sendeku, P. Yu, F.T. Dajan, C. Zhu, N. Li, J. Wang, F. Wang, Z. Wang, J. He, Nanotechnology 32 (47) (2021) 472001.
[11] D. Afanasiev, J.R. Hortensius, B.A. Ivanov, A. Sasani, E. Bousquet, Y.M. Blanter, R.V. Mikhaylovskiy, A.V. Kimel, A.D. Caviglia, Nature Mater. 20 (5) (2021) 607–611.
[12] E. Beaurepaire, J.-C. Merle, A. Daunois, J.-Y. Bigot, Phys. Rev. Lett. 76 (22) (1996) 4250–4253.
[13] J. Hohlfeld, E. Matthias, R. Knorren, K.H. Bennemann, Phys. Rev. Lett. 78 (25) (1997) 4861–4864.
[14] J. Hohlfeld, T. Gerrits, M. Bilderbeek, T. Rasing, H. Awano, N. Ohta, Phys. Rev. B 65 (1) (2001) 012413.
[15] C. Stamm, T. Kachel, N. Pontius, R. Mitzner, T. Quast, K. Holldack, S. Khan, C. Lupulescu, E.F. Aziz, M. Wietstruk, H. Dürr, W. Eberhardt, Nature Mater. 6 10 (2007) 740–743.
[16] H. Liu, J.-T. Sun, C. Cheng, F. Liu, S. Meng, Phys. Rev. Lett. 120 (23) (2018) 237403.
[17] B. Liu, H. Bromberger, A. Cartella, T. Gebert, M. Först, A. Cavalleri, 2017 Conference on Lasers and Electro-Optics, CLEO, 2017, pp. 1–2.
[18] T. Brixner, I.V. Stiopkin, G.R. Fleming, Opt. Lett. 29 (8) (2004) 884.
[19] S.R. Acharya, V. Turkowski, G. Zhang, T.S. Rahman, Phys. Rev. Lett. 125 (1) (2020) 017202.
[20] K. Cai, Z. Zhu, J.M. Lee, R. Mishra, L. Ren, S.D. Pollard, P. He, G. Liang, K.L. Teo, H. Yang, Nat. Electron. 3 (1) (2020) 37–42.
[21] M. Fechner, A. Sukhov, L. Chotorlishvili, C. Kenel, J. Berakdar, N.A. Spaldin, Phys. Rev. Mater. 2 (6) (2018) 064401.
[22] A. Eschenlohr, U. Bovensiepen, J. Phys.: Condens. Matter 30 (3) (2017) 030301.
[23] Z. Chen, L.-W. Wang, Sci. Adv. 5 (6) (2019) eaau8000.
[24] J. Stöhr, H.C. Siegmann, Ultrafast Magnetization Dynamics, Springer, 2006, pp. 679–759,
[25] B. Liu, S. Liu, L. Yang, Z. Chen, E. Zhang, Z. Li, J. Wu, X. Ruan, F. Xiu, W. Liu, L. He, R. Zhang, Y. Xu, Phys. Rev. Lett. 125 (26) (2020) 267205.
[26] S. Zhang, R. Xu, N. Luo, X. Zou, Nanoscale 13 (3) (2021) 1398–1424.
[27] M. Gibertini, M. Koperski, A.F. Morpurgo, K.S. Novoselov, Nature Nanotechnol. 14 (5) (2019) 408–419.
[28] B. Peng, H. Zhang, W. Chen, B. Hou, Z.-J. Qiu, H. Shao, H. Zhu, B. Monserrat, D. Fu, H. Weng, C.M. Soukoulis, Npj 2D Mater. Appl. 4 (1) (2020) 14.
[29] Y. Qi, M. Guan, D. Zahn, T. Vasileiadis, H. Seiler, Y.W. Windsor, H. Zhao, S. Meng, R. Ernstorfer, ACS Nano 16 (7) (2022) 11124–11135.
[30] C. Bao, P. Tang, D. Sun, S. Zhou, Nat. Rev. Phys. 4 (1) (2021) 33–48.
[31] S.A. Owerre, Sci. Rep. 8 (1) (2018) 4431.
[32] M. Suda, R. Kato, H.M. Yamamoto, Science 347 (6223) (2015) 743–746.
[33] M. Budden, T. Gebert, M. Buzzi, G. Jotzu, E. Wang, T. Matsuyama, G. Meier, Y. Laplace, D. Pontiroli, M. Riccò, F. Schlawin, D. Jaksch, A. Cavalleri, Nat. Phys. 17 (5) (2021) 611–618.
[34] A. Cavalleri, Contemp. Phys. 59 (1) (2018) 31–46.
[35] A. de la Torre, D.M. Kennes, M. Claassen, S. Gerber, J.W. McIver, M.A. Sentef, Rev. Modern Phys. 93 (4) (2021) 041002.
[36] S.-Q. Hu, H. Zhao, C. Lian, X.-B. Liu, M.-X. Guan, S. Meng, Npj Quantum Mater. 7 (1) (2022) 14.

[37] M.-X. Guan, X.-B. Liu, D.-Q. Chen, X.-Y. Li, Y.-P. Qi, Q. Yang, P.-W. You, S. Meng, Phys. Rev. Lett. 128 (1) (2022) 015702.
[38] M. Henstridge, M. Först, E. Rowe, M. Fechner, A. Cavalleri, Nat. Phys. 18 (4) (2022) 457–461.
[39] B. Peng, H. Zhang, W. Chen, B. Hou, Z.-J. Qiu, H. Shao, H. Zhu, B. Monserrat, D. Fu, H. Weng, C.M. Soukoulis, Npj 2D Mater. Appl. 4 (1) (2020) 14.
[40] S.A. Owerre, Sci. Rep. 8 (1) (2018) 4431.
[41] D.M. Juraschek, T. Neuman, P. Narang, Phys. Rev. Res. 4 (1) (2022) 013129.
[42] T.F. Nova, A. Cartella, A. Cantaluppi, M. Först, D. Bossini, R.V. Mikhaylovskiy, A.V. Kimel, R. Merlin, A. Cavalleri, Nat. Phys. 13 (2) (2017) 132–136.
[43] D.M. Juraschek, P. Narang, N.A. Spaldin, Phys. Rev. Res. 2 (4) (2020) 043035.
[44] A.S. Disa, T.F. Nova, A. Cavalleri, Nat. Phys. 17 (10) (2021) 1087–1092.
[45] R. G mez-Abal, W. H bner, J. Phys.: Condens. Matter 15 (5) (2003) S709–S722.
[46] R. Gómez-Abal, O. Ney, K. Satitkovitchai, W. Hübner, Phys. Rev. Lett. 92 (22) (2004) 227402.
[47] D. Chen, P. You, Z. Nie, N. Wu, C. Lian, C. Zhang, S. Meng, Chin. Sci. Bull. 66 (24) (2021) 3088–3099.
[48] J. Xu, D. Chen, S. Meng, J. Am. Chem. Soc. 143 (27) (2021) 10382–10388.
[49] C. Lian, M. Guan, S. Hu, J. Zhang, S. Meng, Adv. Theory Simul. 1 (8) (2018) 1800055.
[50] M. Guan, S. Hu, H. Zhao, C. Lian, S. Meng, Appl. Phys. Lett. 116 (4) (2020) 043101.
[51] G.P. Zhang, W. Hübner, Phys. Rev. Lett. 85 (14) (2000) 3025–3028.
[52] G. Zhang, W. Hübner, Appl. Phys. B: Lasers Opt. 68 (3) (1999) 495–499.
[53] B. Koopmans, G. Malinowski, F.D. Longa, D. Steiauf, M. Faehnle, T. Roth, M. Cinchetti, M. Aeschlimann, Nature Mater. 9 3 (2010) 259–265.
[54] B. Koopmans, M. van Kampen, J.T. Kohlhepp, W.J.M. de Jonge, Phys. Rev. Lett. 85 (4) (2000) 844–847.
[55] D.J. Gross, Proc. Natl. Acad. Sci. 93 (25) (1996) 14256–14259.
[56] E.K.U. Gross, N.T. Maitra, Fundamentals of Time-Dependent Density Functional Theory, Springer Berlin Heidelberg, 2012, pp. 53–99.
[57] D. Shin, H. Hübener, U. De Giovannini, H. Jin, A. Rubio, N. Park, Nature Communications 9 (1) (2018) 638.
[58] M. Pashkevich, 2015, http://dx.doi.org/10.13140/RG.2.2.18540.56962, Publisher: Unpublished.
[59] A. Vaterlaus, T. Beutler, F. Meier, Phys. Rev. Lett. 67 (23) (1991) 3314–3317.
[60] W. Hübner, K.H. Bennemann, Phys. Rev. B 53 (6) (1996) 3422–3427, arXiv: cond-mat/9508120.
[61] S. Anisimov, B. Kapeliovitch, T. Perel'man, Sov. Phys.–JETP 39 (1974) 375.
[62] A. Kirilyuk, A.V. Kimel, T. Rasing, Rev. Modern Phys. 82 (3) (2010) 2731–2784.
[63] A. Scholl, L. Baumgarten, R. Jacquemin, W. Eberhardt, Phys. Rev. Lett. 79 (25) (1997) 5146–5149.
[64] W. Hübner, G.P. Zhang, Phys. Rev. B 58 (10) (1998) R5920–R5923.
[65] A.M. Rappe, A. Dal Pino, M. Needels, J.D. Joannopoulos, Phys. Rev. B 46 (12) (1992) 7353–7357.
[66] E. Cappelluti, F. Caruso, D. Novko, Progress Surf. Sci. 97 (3) (2022) 100664.
[67] T. Ostler, J. Barker, R. Evans, R. Chantrell, U. Atxitia, O. Chubykalo-Fesenko, S. El Moussaoui, L. Le Guyader, E. Mengotti, L. Heyderman, F. Nolting, A. Tsukamoto, A. Itoh, D. Afanasiev, B. Ivanov, A. Kalashnikova, K. Vahaplar, J. Mentink, A. Kirilyuk, T. Rasing, A. Kimel, Nature Commun. 3 (1) (2012) 666.
[68] K. Vahaplar, A.M. Kalashnikova, A.V. Kimel, D. Hinzke, U. Nowak, R. Chantrell, A. Tsukamoto, A. Itoh, A. Kirilyuk, T. Rasing, Phys. Rev. Lett. 103 (11) (2009) 117201.
[69] Y. Xu, M. Deb, G. Malinowski, M. Hehn, W. Zhao, S. Mangin, Adv. Mater. 29 (42) (2017) 1703474.
[70] A.S. Disa, M. Fechner, T.F. Nova, B. Liu, M. Först, D. Prabhakaran, P.G. Radaelli, A. Cavalleri, Nat. Phys. 16 (9) (2020) 937–941.
[71] T. Ogasawara, N. Iwata, Y. Murakami, H. Okamoto, Y. Tokura, Appl. Phys. Lett. 94 (16) (2009) 162507.
[72] P. Zhang, T.-F. Chung, Q. Li, S. Wang, Q. Wang, W.L.B. Huey, S. Yang, J.E. Goldberger, J. Yao, X. Zhang, Nature Mater. (2022).
[73] B. Koopmans, J.J.M. Ruigrok, F.D. Longa, W.J.M. de Jonge, Phys. Rev. Lett. 95 (26) (2005) 267207.
[74] B. Hillebrands, K. Ounadjela, Spin Dynamics in Confined Magnetic Structures I. Vol. 83, Springer Science & Business Media, 2003.
[75] G.M. Müller, J. Walowski, M. Djordjevic, G.-X. Miao, A. Gupta, A.V. Ramos, K. Gehrke, V. Moshnyaga, K. Samwer, J. Schmalhorst, A. Thomas, A. Hütten, G. Reiss, J.S. Moodera, M. Münzenberg, Nature Mater. 8 (1) (2009) 56–61.
[76] C.D. Stanciu, A.V. Kimel, F. Hansteen, A. Tsukamoto, A. Itoh, A. Kirilyuk, T. Rasing, Phys. Rev. B 73 (22) (2006) 220402.
[77] D.M. Wang, Y.H. Ren, X. Liu, J.K. Furdyna, M. Grimsditch, R. Merlin, Phys. Rev. B 75 (23) (2007) 233308.
[78] A.V. Kimel, A. Kirilyuk, P.A. Usachev, R.V. Pisarev, A.M. Balbashov, T. Rasing, Nature 435 (7042) (2005) 655–657.
[79] G. Ju, J. Hohlfeld, B. Bergman, R.J.M. van de Veerdonk, O.N. Mryasov, J.-Y. Kim, X. Wu, D. Weller, B. Koopmans, Phys. Rev. Lett. 93 (19) (2004) 197403.
[80] J.-U. Thiele, M. Buess, C.H. Back, Appl. Phys. Lett. 85 (14) (2004) 2857–2859.
[81] F. Pressacco, V. Uhlíř, M. Gatti, A. Nicolaou, A. Bendounan, J.A. Arregi, S.K.K. Patel, E.E. Fullerton, D. Krizmancic, F. Sirotti, Struct. Dyn. 5 (3) (2018) 034501.
[82] A.V. Kimel, A. Kirilyuk, A. Tsvetkov, R.V. Pisarev, T. Rasing, Nature 429 (6994) (2004) 850–853.
[83] S. Tomimoto, M. Matsubara, T. Ogasawara, H. Okamoto, T. Kimura, Y. Tokura, Phys. Rev. Lett. 98 (1) (2007) 017402.
[84] B. Bergman, G. Ju, J. Hohlfeld, R.J.M. van de Veerdonk, J.-Y. Kim, X. Wu, D. Weller, B. Koopmans, Phys. Rev. B 73 (6) (2006) 060407.
[85] P.G. Radaelli, Phys. Rev. B 97 (8) (2018) 085145.